

# AKARI OBSERVATIONS OF BROWN DWARFS. II. CO<sub>2</sub> as Probe of Carbon and Oxygen Abundances in Brown Dwarfs

Takashi Tsuji

*Institute of Astronomy, School of Science, The University of Tokyo,  
2-21-1 Osawa, Mitaka, Tokyo 181-0015, Japan*

ttsuji@ioa.s.u-tokyo.ac.jp

and

Issei Yamamura and Satoko Sorahana<sup>1</sup>

*Institute of Space and Astronautical Science (ISAS), JAXA,  
Yoshino-dai 3-1-1, Chuo-ku, Sagami-hara, Kanagawa 252-5210, Japan*

yamamura@ir.isas.jaxa.jp, sorahana@ir.isas.jaxa.jp

## ABSTRACT

Recent observations with the infrared astronomical satellite *AKARI* have shown that the CO<sub>2</sub> bands at 4.2  $\mu$ m in three brown dwarfs are much stronger than expected from the unified cloudy model (UCM) based on recent solar C & O abundances. This result has been a puzzle, but we now find that this is simply an abundance effect: We show that these strong CO<sub>2</sub> bands can be explained with the UCMs based on the classical C & O abundances ( $\log A_C$  and  $\log A_O$ ), which are about 0.2 dex larger compared to the recent values. Since three other brown dwarfs could be well interpreted with the recent solar C & O abundances, we require at least two model sequences based on the different chemical compositions to interpret all the *AKARI* spectra. The reason for this is that the CO<sub>2</sub> band is especially sensitive to C & O abundances, since the CO<sub>2</sub> abundance depends approximately on  $A_C A_O^2$  — the cube of C & O abundances. For this reason, even low resolution spectra of very cool dwarfs, especially of CO<sub>2</sub>, cannot be understood unless a model with proper abundances is applied. For the same reason, CO<sub>2</sub> is an excellent indicator of C & O abundances, and we can now estimate C & O abundances of brown dwarfs: Three out of six brown dwarfs observed with *AKARI* should have high C & O abundances similar to the classical solar values (e.g.  $\log A_C = 8.60$  and  $\log A_O = 8.92$ ), but the other three may have low C & O abundances similar to the recent solar values (e.g.  $\log A_C = 8.39$  and  $\log A_O = 8.69$ ). This result implies that three out of six brown dwarfs are highly metal rich relative to the Sun if the recent solar C & O abundances are correct.

*Subject headings:* brown dwarfs — infrared: stars — stars: abundances — stars: atmospheres — stars: individual (2MASS J04151954–0935066, 2MASS J05591914–1404488, 2MASS J15232263+3014562, SDSS J053951.99–005902.0, SDSS J083008.12+482847.4, SDSS J144600.60+002452.0) — stars: low-mass

<sup>1</sup>Also at Department of Astronomy, School of Science, The University of Tokyo, Hongo 7-3-1, Bunkyo-ku, Tokyo 113-0033, Japan

## 1. INTRODUCTION

In our recent work, the CO<sub>2</sub> molecule was identified for the first time in the spectra of brown dwarfs observed with the infrared astronomical satellite *AKARI* (Yamamura et al. 2010, here-

after referred to as Paper I). We tried to interpret the observed behavior of the CO<sub>2</sub> band with the use of the model photosphere of brown dwarfs, referred to as the unified cloudy model (UCM; Tsuji 2002, 2005). In modeling the photospheres of brown dwarfs, one problem is how to consider the chemical composition, since no direct abundance analysis is known for brown dwarfs. We thought it reasonable to assume a typical composition for the disk stellar population such as the Sun. However, the solar composition itself experienced drastic changes in the past decades, and the true chemical composition of the Sun is still by no means well established. Nevertheless, we thought it appropriate to use the latest version of the solar abundances as possible proxies for the chemical abundances in the brown dwarfs.

In our earlier version of UCMs (Tsuji 2002), we assumed the solar abundances largely based on the classical LTE analysis using one dimensional (1D) hydrostatic model photospheres and, in particular, C & O abundances were  $\log A_C = 8.60$  and  $\log A_O = 8.92$  on the scale of  $\log A_H = 12.0$  (e.g. Anders & Grevesse 1989; Grevesse et al. 1991). At about the same time as we were computing our first version of UCMs, a new result for the solar C & O abundances based on three dimensional (3D) time-dependent hydrodynamical model of the solar photosphere was published (Allende Prieto et al. 2002). Since the classical 1D model may be too simplified for the real solar photosphere, this new approach seemed to be a useful contribution to the solar abundance analysis. The current version of UCMs (Tsuji 2005) is thus based on this new result ( $\log A_C = 8.39$  and  $\log A_O = 8.69$ ) by Allende Prieto et al. (2002) as noted elsewhere (Tsuji et al. 2004). The new C & O abundances are about 0.2 dex smaller as compared to the classical values referred to above.

We applied our current version of UCMs to the brown dwarfs observed with *AKARI* in Paper I, and we could explain about half of our sample of spectra almost perfectly. For the other half of our targets, we could explain the overall SEDs by this version of UCMs, but we could not explain their strong CO<sub>2</sub> bands. One explanation is that this may be due to an unknown process related to CO<sub>2</sub>, since anomalously strong CO band depths have also been explained by a special process now known as vertical mixing (e.g. Noll et al.

1997; Oppenheimer et al. 1998; Griffith & Yelle 1999; Saumon et al. 2000; Leggett et al. 2007b).

However, we happened to try our old version of UCMs based on the classical C & O abundances and found that the CO<sub>2</sub> band appeared to be much stronger in the spectra based on the old models than on the present models. At the first glance, this is rather surprising because C & O abundances in the old models are only about 0.2 dex larger than those in the present models. However, we realized immediately that the CO<sub>2</sub> abundance is extremely sensitive to both C & O abundances because the CO<sub>2</sub> abundance depends on the cube of C & O abundances ( $A_{CO_2} \propto A_C A_O^2$ ). We recall that the strong dependence of the CO<sub>2</sub> abundance on metallicity,  $[Fe/H]$ <sup>1</sup>, was previously known by a detailed thermochemical analysis of the C, N, and O bearing gaseous molecules (Lodders & Fegley 2002).

The above result demonstrates that at least two different series of model photospheres are needed for the analysis of the CO<sub>2</sub> band observed with *AKARI*. For this purpose, we reconsider our old version of UCMs based on the classical C & O abundances to represent a case of rather high C & O abundances. Our current version of UCMs based on the new C & O abundances will serve as representing a case of the reduced C & O abundances compared to the old version of the UCMs. An important implication of this result is that the metallicity (C & O abundances) in brown dwarfs should have a variety of values.

The interpretation and analysis of the spectra of cool dwarfs already have a rather long history (e.g. Kirkpatrick 2005; Burgasser et al. 2006a; Leggett et al. 2007a; Cushing et al. 2008; Stephens et al. 2009; Yamamura et al. 2010), and the effect of metallicity has been discussed by some authors. For example, Burgasser et al. (2006b) have measured the strengths of the major H<sub>2</sub>O and CH<sub>4</sub> bands in the 1.0–2.5  $\mu$ m region in a large sample of T dwarfs, and found that the resultant spectral indices plotted against spectral type revealed considerable scatter. Several reasons for this result including the effects of dust, gravity, and metallicity have been considered, but it appeared difficult to separate the effect of metallic-

<sup>1</sup>The differential iron abundance of a star relative to the Sun and defined by  $[Fe/H] = \log(A_{Fe}/A_H)_* - \log(A_{Fe}/A_H)_\odot$ .

ity from the remaining parameters. Leggett et al. (2009) have shown that the effect of metallicity on the SEDs of T dwarfs should be significant, but noted that other parameters such as gravity can affect the SEDs similarly. This result again showed the difficulty in determining metallicity uniquely from SEDs. Also, the so-called “blue” L dwarfs classified as L subdwarfs have been interpreted to have low metallicity with  $[\text{Fe}/\text{H}]$  from  $-1.5$  to  $-1.0$  (e.g. Burgasser et al. 2009), but those L dwarfs with unusually blue near-infrared colors can also be explained by a patchy cloud model (Folkes et al. 2007; Marley et al. 2010).

The brief survey outlined above reveals that the problem of metallicity in brown dwarfs is still unresolved. In this paper, we will show clear evidence of metallicity variations in brown dwarfs for the first time. In fact, the most important significance of the discovery of  $\text{CO}_2$  with *AKARI* is that it demonstrated the variations of the C & O abundances by at least 50% in brown dwarfs and that it provided a means by which to estimate the C & O abundances in very cool dwarfs.

In Paper I, we have analyzed the *AKARI* spectra and discussed the basic physical parameters of our objects in detail. There we have applied the conventional method based on a direct comparison of the observed and predicted spectra. In this paper, we examine the results of Paper I by a more detailed numerical method in Section 4.1, and we confirm that the physical parameters determined in Paper I mostly agree with those based on the reduced-chi-square minimization method within the estimated errors. A problem, however, is that an adequate application of such a rigorous numerical method requires the input data of sufficient accuracy. Unfortunately, the input data — our present models of brown dwarfs — are not precise enough for this purpose, as discussed in Section 4.5 of Paper I. Therefore the numerical method does not necessarily provide the best answer and the traditional fitting method “by eye” can still be useful for some cases. For these reasons, we use the physical parameters determined in Paper I and adopt the same approach as Paper I, eye-fitting, throughout this paper.

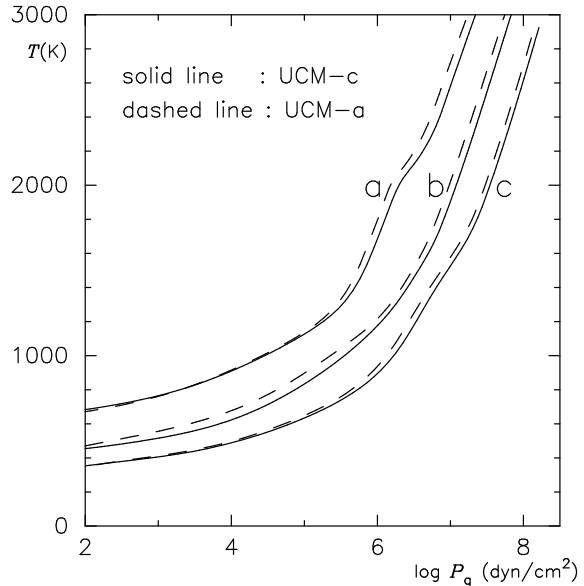


Fig. 1.— The effects of C & O abundances on the thermal structure of cool dwarfs. The solid and dashed lines are based on the 3D and 1D solar abundances (see Table 1), respectively. a)  $T_{\text{eff}} = 1500 \text{ K}$ ,  $T_{\text{cr}} = 1700 \text{ K}$ , and  $\log g = 4.5$ . b)  $T_{\text{eff}} = 1200 \text{ K}$ ,  $T_{\text{cr}} = 1900 \text{ K}$ , and  $\log g = 4.5$ . c)  $T_{\text{eff}} = 900 \text{ K}$ ,  $T_{\text{cr}} = T_{\text{cond}}$ , and  $\log g = 4.5$ .

## 2. ROLE OF THE CARBON AND OXYGEN ABUNDANCES IN THE UCM

Our two series of UCMs are referred to as UCM-a and UCM-c, and they only differ in C & O abundances as summarized in Table 1. The UCM-a series is based on the classical C & O abundances, which we refer to as 1D solar abundances for simplicity, and the UCM-c series on the new abundances, which we refer to as 3D solar abundances.

We first examine the effects of C & O abundances on the thermal structure of the photosphere. For this purpose, the models of the UCM-c series are taken from our database<sup>2</sup>. Since our code to compute UCMs has been modified to some extent over the last 10 years, we recompute all the models of the UCM-a series used in the present

<sup>2</sup>The numerical details of this version (UCM-c series) are available from <http://www.mtk.ioa.s.u-tokyo.ac.jp/~ttsuji/export/ucmLM/and/ucm/>.

Table 1: Carbon and Oxygen Abundances in UCMs

series	$\log A_C^a$	$\log A_O^a$	Note on chemical composition
UCM-a	8.60	8.92	1D solar abundances (e.g. Anders & Grevesse 1989) <sup>b</sup>
UCM-c	8.39	8.69	3D solar abundances (e.g. Allende Prieto et al. 2002) <sup>c</sup>

Notes.

a) The logarithmic abundance on the scale of  $\log A_H = 12.0$ . b) Actually, we have applied a slightly updated version as summarized in Table 1 of Tsuji (2002). c) A full listing of the abundances is given in <http://www.mtk.ioa.s.u-tokyo.ac.jp/~ttsuji/export/ucm/tables/table1.dat>.

paper. Therefore the models of the UCM-a and UCM-c series are now computed by exactly the same code, except for the Rosseland and Planck mean opacities, which of course differ according to the chemical composition adopted.

We show a simple comparison of the photospheric structures of the UCM-a and UCM-c series for the cases of  $T_{\text{eff}} = 900, 1200$ , and  $1500$  K in Figure 1. Other parameters such as  $T_{\text{cr}}$  and  $\log g$  are chosen to be those actually found for our objects (see Table 2). Inspection of Figure 1 reveals that the models of the UCM-a series shown by the dashed lines are generally warmer by up to about 100 K as compared to the models of the UCM-c series shown by the solid lines. Since the major opacity sources such as CO and H<sub>2</sub>O are more abundant in the UCM-a than in the UCM-c series, the blanketing effect due to molecular bands should be more effective and hence the models of the UCM-a series are warmer than those of the UCM-c series.

Next, we examine the effects of C & O abundances on the CO<sub>2</sub> and other molecular abundances. We present the abundances of H<sub>2</sub>O, CO, CO<sub>2</sub>, and CH<sub>4</sub> for the case of  $T_{\text{eff}} = 1500$  K,  $T_{\text{cr}} = 1700$  K, and  $\log g = 4.5$  for the models of the UCM-c (applied to 2MASS J152322+3014 in Section 3) and UCM-a (applied to SDSS J083008+4828) series in Figure 2 as the solid and dashed lines, respectively. The increased C & O abundances result in the increases of CO, CO<sub>2</sub>, and H<sub>2</sub>O abundances as expected. The increase of the CO<sub>2</sub> abundance in the UCM-a series is quite

significant for the reason noted before. On the contrary, the CH<sub>4</sub> abundance shows a decrease in the UCM-a series and this unexpected result may be because the direct effect of the increased carbon abundance on the CH<sub>4</sub> abundance is superseded by the dissociation of CH<sub>4</sub> due to the elevated temperatures in the model of the UCM-a series (Figure 1).

As another example, we show the case of  $T_{\text{eff}} = 1200$  K,  $T_{\text{cr}} = 1900$  K, and  $\log g = 4.5$  in Figure 3. The results are again shown for the UCM-c and UCM-a series with the solid and dashed lines, respectively. In this case, the effects of the abundance changes are more pronounced, especially for CO<sub>2</sub>. We will see in Section 3 that the case of the UCM-a series is approximately realized in 2MASS J055919–1404 in which the CO<sub>2</sub> band appears to be very strong.

### 3. EFFECTS OF THE CARBON AND OXYGEN ABUNDANCES ON THE SPECTRA OF BROWN DWARFS

We compare the observed spectra of six brown dwarfs with the predicted ones based on the models of the UCM-a and UCM-c series in Figure 4 (a)–(f). The effect of C & O abundances on the spectra of brown dwarfs can be seen most clearly in a comparison of 2MASS J152322+3014 and SDSS J083008+4828 shown in Figure 4(c) and Figure 4(d), respectively. These two brown dwarfs were found to have nearly the same physical parameters ( $T_{\text{eff}} = 1500$  K,  $T_{\text{cr}} = 1700$  K, and  $\log g = 4.5$ ) but the spectra looked to be quite dif-

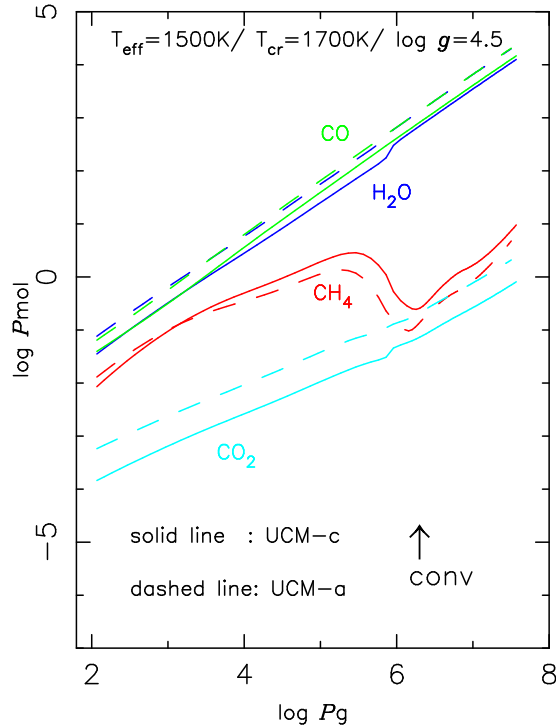


Fig. 2.— The effects of C & O abundances on the molecular abundances in cool dwarfs. The solid and dashed lines are based on the 3D and 1D solar abundances (see Table 1), respectively. The physical parameters of the model are:  $T_{\text{eff}} = 1500 \text{ K}$ ,  $T_{\text{cr}} = 1700 \text{ K}$ , and  $\log g = 4.5$ . This case may apply to 2MASS J152322+3014 (solid line) and SDSS J083008+4828 (dashed line). The units of  $P_g$  and  $P_{\text{mol}}$  are  $\text{dyn cm}^{-2}$ . The arrow indicates the onset of convection.

ferent (Paper I). In particular, the  $\text{CO}_2$  band at  $4.2 \mu\text{m}$  appeared to be much stronger in SDSS J083008+4828 than in 2MASS J152322+3014. In 2MASS J152322+3014, the observed spectrum could be accounted for by the model of the UCM-c series (Paper I), as confirmed by curve 1 in Figure 4(c): Especially, the regions of the  $\text{H}_2\text{O}$   $2.7 \mu\text{m}$  and the  $\text{CO}_2$   $4.2 \mu\text{m}$  bands as well as the  $Q$ -branch of  $\text{CH}_4$  band appeared to be well explained by the model of the UCM-c series. On the other hand, the predicted spectrum based on the model of the UCM-a series shown by curve 2 can not explain those features.

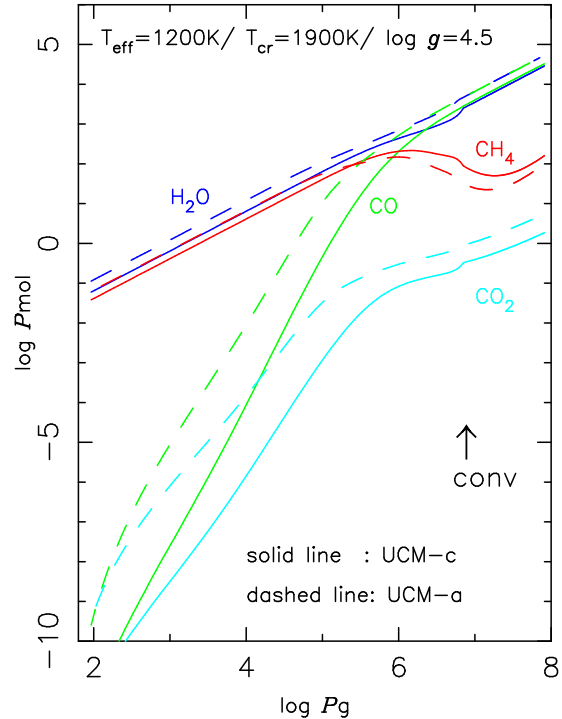


Fig. 3.— The same as Figure 2 but for the physical parameters of the model:  $T_{\text{eff}} = 1200 \text{ K}$ ,  $T_{\text{cr}} = 1900 \text{ K}$ , and  $\log g = 4.5$ . This case may apply to 2MASS J055919–1404 (dashed line).

In SDSS J083008+4828 shown in Figure 4(d), the observed spectrum could not be accounted for by the model of the UCM-c series (Paper I), as confirmed by curve 1. On the other hand, the strong  $\text{CO}_2$  band at  $4.2 \mu\text{m}$  can now be explained reasonably well by the model of the UCM-a series, as shown by curve 2 in Figure 4(d). Thus the large depression due to the  $\text{CO}_2$  band turns out to be due to the high C & O abundances in a LTE model. It is to be noted that this result is due to the increase of both C & O abundances. In fact, a change of the C abundance alone, for example, produced only minor change on the  $\text{CO}_2$  band strength (Paper I). The large depression over the  $2.7 \mu\text{m}$  region mostly due to  $\text{H}_2\text{O}$  can also be better explained with the model of the UCM-a series. On the contrary, the  $Q$ -branch of the  $\text{CH}_4$  band appears to be weaker with the model of the UCM-a than with that of the UCM-c series, consistent

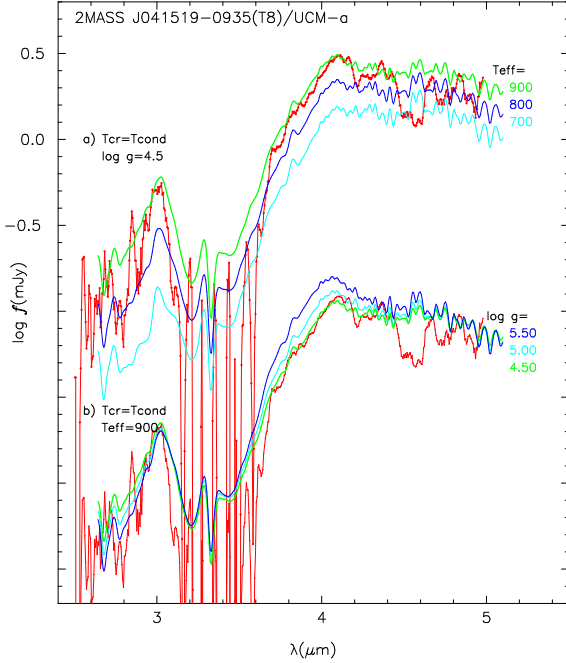


Fig. 5.— Observed spectrum of 2MASS J041519–0935 is compared with the predicted spectra based on the models of the UCM-a series. The best fit is obtained for  $T_{\text{eff}} = 900$  K,  $T_{\text{cr}} = T_{\text{cond}}$ , and  $\log g = 4.5$ . a) Effect of  $T_{\text{eff}}$  under the fixed values of  $T_{\text{cr}} = T_{\text{cond}}$  and  $\log g = 4.5$ . b) Effect of  $\log g$  under the fixed values of  $T_{\text{eff}} = 900$  K and  $T_{\text{cr}} = T_{\text{cond}}$ .

with the decrease of the  $\text{CH}_4$  in the UCM-a compared to the UCM-c series (Figure 2). Also, the observed  $\text{CH}_4$   $Q$ -branch indeed agrees better with the predicted one based on the model of UCM-a. Thus, we conclude that the UCM-a series should be applied to SDSS J083008+4828 rather than the UCM-c series.

In Figure 4(a), we compare the observed spectrum of SDSS J053952–0059 with the predicted ones based on the models of the UCM-a and UCM-c series. We already know that this spectrum is well explained by a model of UCM-c series in Paper I (curve 1). On the other hand, the observed spectrum cannot be explained by a model of the UCM-a series of the same parameters (curve 2). We obtain more or less similar result for SDSS J144600+0024, namely the observed spectrum of this object can be well explained by the model of

the UCM-c (curve 1 in Figure 4(b)), but not with that of the UCM-a series (curve 2).

In Figure 4(e), we examine the case of 2MASS J055919–1404 in which the observed  $\text{CO}_2$  band is very strong. We could not explain the  $\text{CO}_2$  and  $\text{CO}$  bands in this object with our UCM-c series (Paper I), as confirmed by curve 1. But we can now explain the strong  $\text{CO}_2$  band approximately with our model of the UCM-a series, as shown by curve 2. This result is fairly consistent with the very large increase of the  $\text{CO}_2$  abundance for this model as noted in Figure 3. The fit of curve 2 based on the UCM-a series can in principle be improved further by a fine tuning of C & O abundances. But we defer such a detailed abundance analysis to future works and we only note here that the strength of the  $\text{CO}_2$  band is adjustable by changing C & O abundances.

Lastly, we examine the case of 2MASS J041519–0935 in Figure 4(f). This is a case in which the fitting parameters had to be changed from the result of Paper I: We previously found that  $T_{\text{eff}} = 800$  K based on the model of the UCM-c series. However, the  $\text{H}_2\text{O}$  band at  $2.7 \mu\text{m}$  appears to be too strong if we apply the same parameters to the model of the UCM-a series. As shown in Figure 5(a), the observed spectrum can be explained by the model of a higher effective temperature of  $T_{\text{eff}} = 900$  K with the model of the UCM-a series. Also, we find that the case of  $\log g = 4.5$  provides the best fit as shown in Figure 5(b). Thus, we conclude that  $(T_{\text{eff}}, T_{\text{cr}}, \log g) = (900, T_{\text{cond}}, 4.5)$  for 2MASS J041519–0935 for the models of the UCM-a series. We show the best possible predicted spectrum based on the model of the UCM-c series with  $T_{\text{eff}} = 800$  K and that based on the model of the UCM-a series with  $T_{\text{eff}} = 900$  K by curve 1 and curve 2, respectively, in Figure 4(f). We see that the model of the UCM-a series appears to match better with the observed spectrum than the model of the UCM-c series.

Finally, we summarize the basic parameters of the six brown dwarfs in Table 2. The major change from Table 4 of Paper I is to have introduced abundance classes in column 3 indicated by the UCM series applied : UCM-a and UCM-c means that C & O abundances should be close to those of the 1D and 3D solar abundances, respectively. The physical parameters are re-examined with the models of the UCM-a series in the same manner

Table 2: Basic Parameters from the Model Fittings by Using UCMs

no.	object	UCM series <sup>a</sup>	$T_{\text{eff}}$ (K)	$T_{\text{cr}}$ (K)	$\log g$	$R/R_J^b$	$\Delta T_{\text{eff}}$ (K) <sup>c</sup>
1	SDSS J053952–0059	UCM-c	1800	1800	5.5	0.804	–110
2	SDSS J144600+0024	UCM-c	1700	1700	4.5	0.716	–108
3	2MASS J152322+3014	UCM-c	1500	1700	4.5	0.684	–170
4	SDSS J083008+4828	UCM-a	1500	1700	4.5	0.610	–173
5	2MASS J055919–1404	UCM-a	1200	1900	4.5	1.122	–269
6	2MASS J041519–0935	UCM-a	900	$T_{\text{cond}}$	4.5	0.676	–136

Notes.

a) The UCM series applied and indicates approximate C & O abundances (see Table 1). b) Radius  $R$  relative to the Jupiter’s radius  $R_J$ . c)  $\Delta T_{\text{eff}} = T_{\text{eff}}$  (empirical values by Vrba et al. (2004)) –  $T_{\text{eff}}$  (column 4 in this Table).

as in Paper I. A major change in physical parameter is  $T_{\text{eff}}$  for 2MASS J041519–0935, which is changed from 800 K to 900 K as shown in Figure 5(a). As for other five objects, the physical parameters for the models of the UCM-a series remain the same as for the UCM-c series. We confirm that the overall SEDs based on the models of the UCM-a and UCM-c series of the same physical parameters agree well (see Figure 4) even though some local features due to the CO<sub>2</sub> and H<sub>2</sub>O bands differ somewhat. Thus, it is natural that the physical parameters mainly derived from the fits of the overall SEDs remain the same for UCM-a and UCM-c series. The  $R/R_J$  values for SDSS J083008+4828, 2MASS J055919–1404, and 2MASS J041519–0935 are changed slightly, reflecting the changes of models from the UCM-c to the UCM-a series.

## 4. DISCUSSION

### 4.1. Validity of our “best fit” models

Fitting of the model spectra to the observed spectra is carried out by “eyes” throughout in this paper as well as Paper I. The reader might wonder whether the eye-fitting can find reliable “best” models for various objects. In this subsection we assess our eye-fitting by comparing with the numerical fitting results.

We evaluate the goodness of fit by the reduced-chi-square (hereafter  $\mathcal{R}$ ) defined as,

$$\mathcal{R} = \sum_{i=1}^N \left( \frac{f_i - CF_i}{\sigma_i} \right)^2 / (N - m), \quad (1)$$

where  $f_i$  and  $F_i$  are fluxes of the observed and model spectra at  $i$ -th wavelength grid, respectively. The uncertainty of the observed flux is indicated as  $\sigma_i$ , and  $m$  is the degree of freedom.  $C$  is the scaling factor that minimizes  $\mathcal{R}$  and is given by

$$C = \frac{\sum f_i F_i / \sigma_i^2}{\sum F_i^2 / \sigma_i^2}. \quad (2)$$

These definitions are in principle equivalent to “Goodness-of-fit” statistics  $G$  by Cushing et al. (2008) for the equal weight case.

From our experience in Paper I we know that the current UCM cannot fit the observations beyond  $4 \mu\text{m}$  at least in some objects. Therefore we limit the wavelength range for calculating  $\mathcal{R}$  to  $2.64\text{--}4.15 \mu\text{m}$  (cf. Model spectra are available from  $2.64 \mu\text{m}$  and CO<sub>2</sub> band starts from  $4.17 \mu\text{m}$ ).

In Table 3 we list the three best models based on the  $\mathcal{R}$  value and the model quoted in Paper I (by eye-fitting) for each object in our sample. The eye-fitting results are indicated in bold-face. The models selected by the eye-fitting achieve the minimum  $\mathcal{R}$  for SDSS J053951–0059 (L5) and

Table 3: The Best Three Models According to the Numerical Fitting.

No.	$T_{\text{eff}}$ (K)	$\log g$	$T_{\text{cr}}$ (K)	$C$ ( $\times 10^6$ )	$\mathcal{R}$
SDSS J053951–0059 (L5)					
<b>1</b>	<b>1800</b>	<b>5.5</b>	<b>1800</b>	<b>6.32</b>	<b>1.127</b>
2	1900	5.5	1800	5.82	1.206
3	1900	5.0	1800	6.37	1.288
SDSS J144600+0024 (L5)					
1	2000	4.5	1700	1.53	0.496
2	1900	4.5	1700	1.61	0.513
3	1800	4.5	1700	1.69	0.553
<b>10</b>	<b>1700</b>	<b>4.5</b>	<b>1700</b>	<b>1.79</b>	<b>0.695</b>
2MASS J152322+3014 (L8)					
1	1600	5.5	1700	1.89	0.675
2	1600	5.0	1700	1.91	0.733
3	1700	5.5	1800	1.69	0.740
<b>4</b>	<b>1500</b>	<b>4.5</b>	<b>1700</b>	<b>2.45</b>	<b>0.793</b>
SDSS J083008+4828 (L9)					
1	1600	4.5	1800	3.78	0.679
2	1700	4.5	1800	3.52	0.711
3	1800	5.0	1900	3.44	0.746
<b>9</b>	<b>1500</b>	<b>4.5</b>	<b>1700</b>	<b>4.54</b>	<b>0.841</b>
2MASS J055919–1404 (T4.5)					
1	1200	4.5	$T_{\text{cond}}$	21.8	0.389
<b>2</b>	<b>1200</b>	<b>4.5</b>	<b>1900</b>	<b>20.3</b>	<b>0.418</b>
3	1100	4.5	1700	25.3	0.482
2MASS J041519–0935 (T8)					
<b>1</b>	<b>800</b>	<b>4.5</b>	$T_{\text{cond}}$	<b>29.1</b>	<b>0.170</b>
2	900	4.5	$T_{\text{cond}}$	20.6	0.173
3	900	5.0	$T_{\text{cond}}$	17.2	0.195

Notes.

Models of the UCM-c series are adopted throughout as in Paper I. The eye-fitting results quoted from Paper I are indicated in bold-face.

2MASS J041519–0935 (T8; for this particular object we search for the best model among those of  $T_{\text{cr}} = T_{\text{cond}}$  for the reason outlined in Section 4.3.6 of Paper I) and the second minimum  $\mathcal{R}$  for 2MASS J055919–1404 (T4.5). The difference of  $\mathcal{R}$  between the first and second model for the last case is tiny, and the model parameters are within the uncertainty we stated in Paper I ( $\pm 100$  K for  $T_{\text{eff}}$  and  $T_{\text{cr}}$ , and  $\pm 0.5$  dex for  $\log g$ ).

For two late-L objects, 2MASS J152322+3014 (L8) and SDSS J083008+4828 (L9), the differences in the model parameters are mostly within the uncertainty of eye-fitting, although the models used in Paper I are not included in the numerical best three for these dwarfs. Although  $\log g$  of 2MASS J152322+3014 differs by 1.0 dex, the eye-selected model is in the 4th position in the list, and we consider that it is still in the accepted range.

A significant difference between the two methods is found in the L5 dwarf SDSS J144600+0024. The numerical fitting suggests  $T_{\text{eff}} = 2000$  K as the best, which is 300 K higher than the one selected by the eye-fitting. The second and third are of  $T_{\text{eff}} = 1900$  and 1800 K.  $\log g$  and  $T_{\text{cr}}$  are the same in all four models. In fact we regarded such high  $T_{\text{eff}}$  values to be unrealistic for an L5 dwarf, and did not consider them in the eye-fitting. The empirical  $T_{\text{eff}}$  derived by Vrba et al. (2004) of this object is even low as 1592 K. A key feature is the  $\text{CH}_4$   $3.3\mu\text{m}$  band, which appears only in the  $T_{\text{eff}} = 1700$  K model. The observed spectrum of this source is rather noisy and the detection of this band is marginal. If the tiny dip seen near  $3.3\mu\text{m}$  in the observed spectrum is actually the  $\text{CH}_4$  band, the eye-fitting results, even if it is not perfect, are justified.

The nature of mid-L to early-T type dwarfs are still under debate and their effective temperatures might actually spread to higher values. Incomplete atmosphere modeling is another possible reason. As we discuss in Paper I, current atmosphere models for brown dwarfs are still exploratory and the UCM is one of such models. There are many physical and chemical processes not yet understood in brown dwarfs. These problems shall be attacked and eventually incorporated into future model atmospheres, but it is beyond the scope of the current paper. In addition, some of our *AKARI* spectra have relatively low S/N. Under such circumstances, numerical fitting may not al-



ways return a unique and physically reasonable solution. On the other hand the eye-fitting would give weight to some key features and consider balance over the wavelength range. Our goal in this paper is to highlight the effects of chemical abundance in the brown dwarf atmosphere. The comparisons described above well demonstrate that the eye-fitting is, even if it is not perfect, useful to find reasonable models for our purpose. Therefore, we apply the model parameters based on our eye-fitting for the six objects including J144600+0024 in the analysis throughout this paper.

It is noted that the differences between the models appear much more prominently over the shorter wavelength range especially in  $J$ -band, even if the spectra in the *AKARI* wavelength range are similar to each other. Consideration of near-infrared data such as 2MASS photometry or ground-based spectroscopy will enable constraining the model parameters better (Sorahana et al. in preparation). Such improvements in spectral range will also help us to evaluate the goodness of the fit in the wavelengths beyond  $4\mu\text{m}$ .

#### 4.2. C & O Abundances in Brown Dwarfs

The very strong  $\text{CO}_2$  feature observed with *AKARI* in some brown dwarfs has remained a puzzle (Paper I), but we find that this is simply due to the effect of C & O abundances. Generally, a small change in the chemical composition does not have a large effect on the predicted spectra at low resolution nor on the thermal structure of the photosphere in hotter stars. In fact, this is the reason why one dimensional spectral classification (e.g. Harvard system) is possible for such stars. But in the case of cool stars, a small change of the chemical composition is amplified in molecular abundances. A drastic example is the spectral branching of cool giant stars into M, S, and C types according to whether the C/O ratio is smaller or larger than unity. In cool dwarfs, the change of C & O abundances also produces significant effect on the strengths of molecular bands as well as on the photospheric structures because of the large molecular opacities.

The results of Section 3 reveal that half of the brown dwarf spectra observed with *AKARI* (i.e. SDSS J053952–0059, SDSS J144600+0024, and 2MASS J152322+3014) can be fitted by the predicted spectra based on the models of the UCM-

c series (Paper I). Although the fits are by no means perfect, the fits with the predicted spectra based on the UCM-c series are better than those based on the UCM-a series. For this reason, C & O abundances in these three brown dwarfs should be closer to the recent 3D solar abundances rather than to the classical 1D solar abundances. On the other hand, the remaining half (i.e. SDSS J083008+4828, 2MASS J055919–1404, and 2MASS J041519–0935) of our sample can be reasonably accounted for by the models of the UCM-a series. Therefore, C & O abundances in these three objects should be closer to the classical 1D solar abundances rather than to the recent 3D solar abundances.

Since  $[\text{Fe}/\text{H}]$  of the main sequence stars in the Galactic disk covers the range from  $-0.8$  to  $+0.2$  (e.g. Edvardsson et al. 1993), the same metallicity distribution may apply to brown dwarfs. It is certainly only by chance that the brown dwarfs we have observed are divided into two groups by C & O abundances. Our sample is too small to investigate the metallicity distribution in brown dwarfs, and we hope that this problem can be pursued further with a larger sample.

The problem of the solar C & O abundances is still under intensive discussion (e.g. Ayres et al. 2006; Caffau et al. 2008; Asplund et al. 2009). Although our problem here is not the solar composition, it is of some interest to know which of the proposed solar composition results more realistic for the Sun. If the recent 3D result is more realistic for the Sun, three of our sample may have about solar composition and the remaining three may be about 0.2 dex more metal rich. This means that the proportion of metal rich objects with the highest  $[\text{Fe}/\text{H}]$  of about  $+0.2$  is quite high in our present sample of brown dwarfs.

#### 4.3. Effects of C & O abundances on the $0.9\text{--}2.5\mu\text{m}$ spectra

We have shown that C & O abundances have significant effects on the  $2.5\text{--}5.0\mu\text{m}$  spectra of brown dwarfs, and we now examine their effect on the  $0.9\text{--}2.5\mu\text{m}$  spectra. As examples, we compare the predicted  $0.9\text{--}2.5\mu\text{m}$  spectra of the models of UCM-a and UCM-c series for the case of  $T_{\text{cr}} = 1700\text{K}$ ,  $T_{\text{eff}} = 1500\text{K}$ , and  $\log g = 4.5$ , together with those for the  $2.5\text{--}5.0\mu\text{m}$  spectra in Figure 6. The major difference between the UCM-

a and UCM-c series is that  $\text{H}_2\text{O}$  bands at 1.1, 1.4, 1.9, and  $2.7\mu\text{m}$  are all stronger in the UCM-a (curve 2 in Figure 6) than in the UCM-c series (curve 1), and this is due to a direct effect of the increased oxygen abundance (see Figure 2).

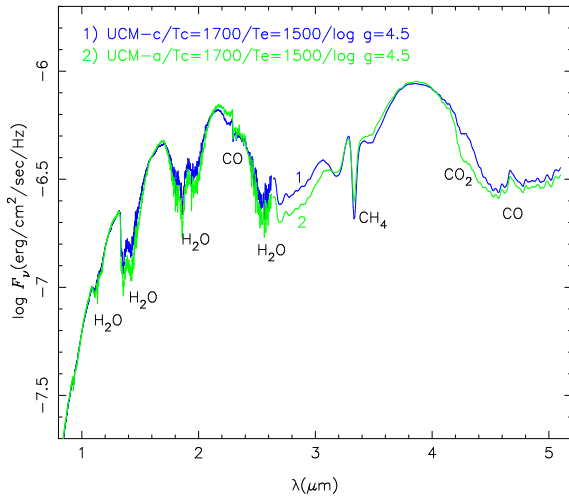


Fig. 6.— Comparison of the predicted spectra based on the models of the UCM-a and UCM-c series for the case of  $T_{\text{cr}} = 1700\text{ K}$ ,  $T_{\text{eff}} = 1500\text{ K}$ , and  $\log g = 4.5$ . The  $0.9\text{--}2.5\mu\text{m}$  spectrum is convolved with the slit function of  $\text{FWHM} = 500\text{ km s}^{-1}$  (a typical resolution of observed spectra in this region), and the  $2.5\text{--}5.0\mu\text{m}$  spectrum with that of  $\text{FWHM} = 3000\text{ km s}^{-1}$  (the resolution of *AKARI* spectra).

Thus the  $\text{H}_2\text{O}$  band strengths depend sensitively on oxygen abundance, and we may hope to determine oxygen abundance from the  $\text{H}_2\text{O}$  bands. However, we must remember that the  $\text{H}_2\text{O}$  band strengths also depend on other parameters such as  $T_{\text{cr}}$ ,  $T_{\text{eff}}$ , and  $\log g$ , and we should encounter the same difficulty due to a degeneracy of the parameters as noted before by other authors (e.g. Burgasser et al. 2006b; Leggett et al. 2009). This fact reconfirms the unique role of  $\text{CO}_2$  as a metallicity (C & O abundances) indicator in brown dwarfs.

## 5. CONCLUDING REMARKS

Thanks to the *AKARI* spectra, we are for the first time able to demonstrate that the metallicity, more specifically C & O abundances, are impor-

tant parameters to understand brown dwarf atmospheres. Until now, we have assumed that it was sufficient to use one sequence of model photospheres based on a representative chemical composition in analyzing low resolution spectra of cool dwarfs. We must now admit that such an assumption is inappropriate, and we should consider abundance effects more carefully, especially of C & O, in our future analysis of cool dwarfs. Also, we cannot use any solar composition for cool dwarfs unless this substitution can be justified by a direct analysis of the spectra of cool dwarfs.

It is true that a detailed abundance analysis of brown dwarfs is difficult especially with low resolution spectra, but well defined molecular bands, even at low resolution, can be potential abundance indicators. We know already that  $\text{CO}_2$  is a fine indicator of C & O abundances. Unfortunately, however,  $\text{CO}_2$  is accessible only from space telescopes and, moreover, spectroscopic observations in the near infrared are mostly neglected by the recent space infrared missions. From the view point of the study on cool dwarfs (and other cool stars), the importance of observing the near infrared spectra (especially between  $2.5$  and  $5.0\mu\text{m}$ ) from space cannot be emphasized too much.

Although the spectra of brown dwarfs appear to be complicated, we are now convinced that the spectra of brown dwarfs can basically be understood on the basis of the LTE model photospheres, but only if the chemical composition is properly considered. This is a reasonable result for such high density photospheres as of brown dwarfs in which frequent collisions easily maintain thermal equilibrium. Thus the chemical composition is the most important ingredient in the interpretation and analysis of even low resolution spectra. Now, with better observed data for brown dwarfs including those from space, analysis of the spectra and abundance determination can be done iteratively for brown dwarfs as for ordinary stars.

Finally, we must remember that a major difficulty in the analysis of the spectra of brown dwarfs is that we have no model of comparable accuracy as for ordinary stars yet. For this reason, even the accurate numerical method such as outlined in Section 4.1 cannot be infallible. In fact, we have no model reproducing all the observable features correctly, and the model found by the numerical method as well as by the eye-

fitting method may prove incorrect even if they are relatively satisfactory among the models currently available. Within this limitation, we hope that our main results on the differential effects of C & O abundances are relatively free of present brown dwarf model uncertainties.

We thank an anonymous referee for critical reading of the text and for invaluable suggestions regarding the method of analysis of the spectra of brown dwarfs. We are grateful to Dr. Poshak Gandhi for his careful checking of the manuscript and many suggestions to improve the text. This research is based on observations with *AKARI*, a JAXA project with the participation of ESA. We acknowledge JSPS/KAKENHI(C) No.22540260 (PI: I. Yamamura).

## REFERENCES

- Allende Prieto, C., Lambert, D. L., & Asplund, M. 2002, *ApJ*, 573, L137
- Anders, E., & Grevesse, N. 1989, *Geochimi. Cosmochimi. Acta*, 53, 197
- Asplund, M., Grevesse, N., Sauval, A. J., & Scott, P. 2009, *ARA&A*, 47, 481
- Ayres, T. R., Plymate, C., & Keller, C. U. 2006, *ApJS*, 165, 618
- Burgasser, A. J., Burrows, A., & Kirkpatrick, J. D. 2006a, *ApJ*, 639, 1095
- Burgasser, A. J., Geballe, T. R., Leggett, S. K., Kirkpatrick, J. D., & Golimowski, D. A. 2006b, *ApJ*, 637, 1067
- Burgasser, A. J., Witte, S., Helling, C., Sanderson, R. E., Bochanski, J. J., & Hauschildt, P. H. 2009, *ApJ*, 697, 148
- Caffau, E., Ludwig, H.-G., Steffen, M., Ayres, T. R., Bonifacio, P., Cayrel, R., Freytag, B., & Plez, B. 2008, *A&A*, 488, 1031
- Cushing, M. C., et al. 2008, *ApJ*, 678, 1372
- Edvardsson, B., Andersen, J., Gustafsson, B., Lambert, D. L., Nissen, P. E., & Tomkin, J. 1993, *A&A*, 275, 101
- Folkes, S. L., Pinfield, D. J., Kendall, T. R., & Jones, H. R. A. 2007, *MNRAS*, 378, 901
- Grevesse, N., Lambert, D. L., Sauval, A. J., van Dishoeck, E. F., Farmer, C. B., & Norton, R. H. 1991, *A&A*, 242, 488
- Griffith, C. A., & Yelle, R. V. 1999, *ApJ*, 519, L85
- Kirkpatrick, J. D. 2005, *ARA&A*, 43, 195
- Leggett, S. K., et al. 2009, *ApJ*, 695, 1517
- Leggett, S. K., Marley, M. S., Freedman, R., Saumon, D., Lie, M. C., Geballe, T. R., Golimowski, D. A., & Stephens, D. C. 2007a, *ApJ*, 667, 537
- Leggett, S. K., Saumon, D., Marley, M. S., Geballe, T. R., & Fan, X. 2007b, *ApJ*, 655, 1079
- Lodders, K., & Fegley, B. 2002, *Icarus*, 155, 393
- Marley, M. S., Saumon, D., & Goldblatt, C. 2010, *ApJ*, 723, L117
- Noll, K. S., Geballe, T. R., & Marley, M. S. 1997, *ApJ*, 489, L87
- Oppenheimer, B. R., Kulkarni, S. R., Matthews, K., & van Kerkwijk, M. H. 1998, *ApJ*, 502, 932
- Saumon, D., Geballe, T. R., Leggett, S. K., Marley, M. S., Freedman, R. S., Lodders, K., Fegley, B., Jr., & Sengupta, S. K. 2000, *ApJ*, 541, 374
- Stephens, D. C., et al. 2009, *ApJ*, 702, 154
- Tsuji, T. 2002, *ApJ*, 575, 264
- Tsuji, T. 2005, *ApJ*, 621, 1033
- Tsuji, T., Nakajima, T., & Yanagisawa, K. 2004, *ApJ*, 607, 511
- Vrba, F. J. et al. 2004, *AJ*, 127, 2948
- Yamamura, I., Tsuji, T., & Tanabé, T. 2010, *ApJ*, 722, 682 (Paper I)

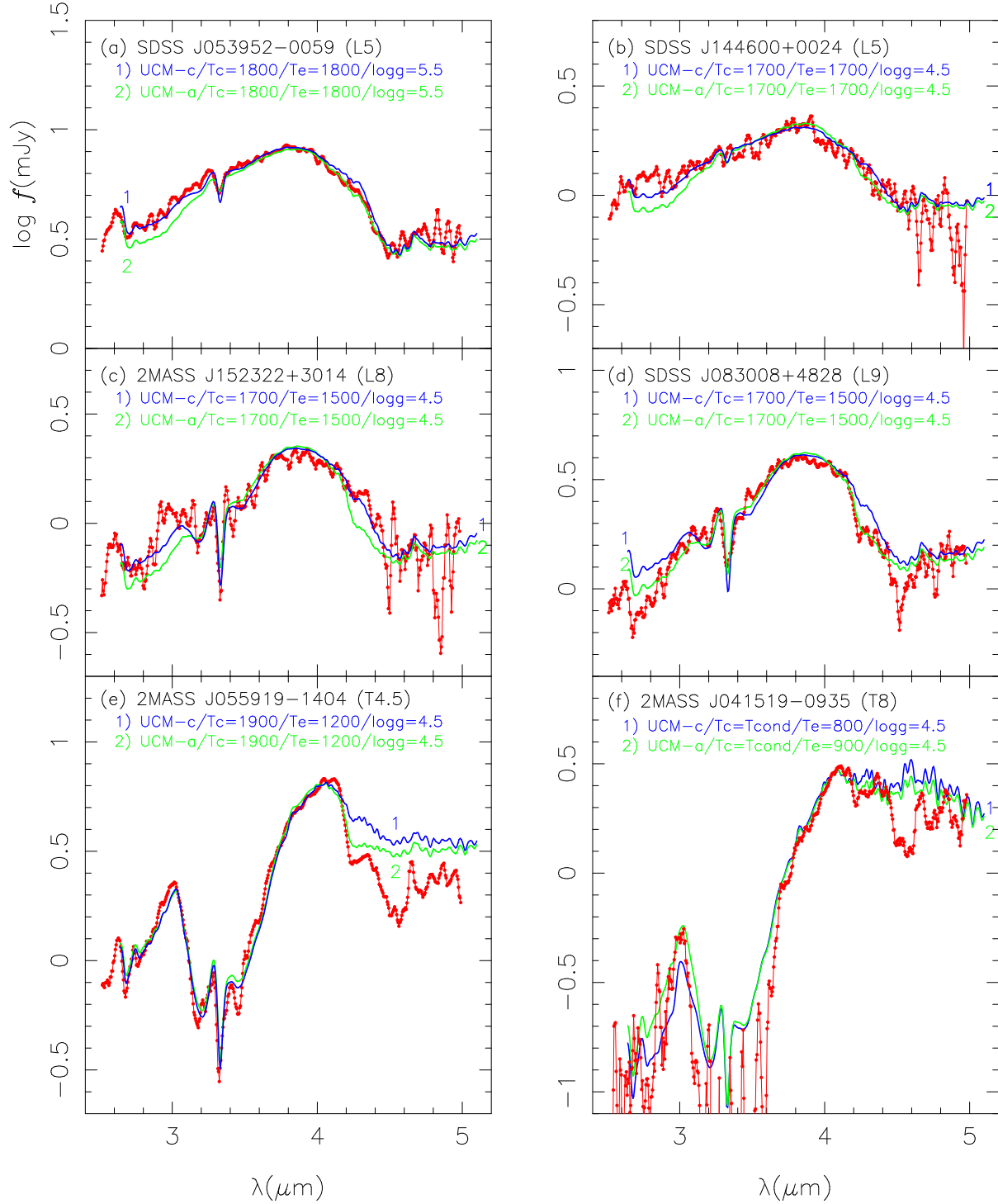


Fig. 4.— Spectra observed with *AKARI* are compared with the predicted spectra based on the models of the UCM-c (curve 1, blue) and UCM-a (curve 2, green) series. The UCM-a series is based on the classical solar C & O abundances (1D abundances, see Table 1) and the UCM-c series on the more recent solar C & O abundances (3D abundances, see Table 1). Note that the brown dwarfs shown in (a), (b), and (c) are relatively well fitted by the models of the UCM-c series while those in (d), (e), and (f) are better described by the models of the UCM-a series.